 doi:10.20944/preprints202207.0089.v1

Article

Nusselt Numbers and Friction Factor determination of Air-Side Finned Heat Exchangers – Individual Correlations of Each Row

Mateusz Marcinkowski *, Dawid Taler, Jan Taler and Katarzyna Węglarz

Faculty of Environmental Engineering and Energy, Cracow University of Technology, 31-155 Cracow, Poland; dawid.taler@pk.edu.pl (D.T.); jan.taler@pk.edu.pl (J.T.); katarzyna.weglarz@pk.edu.pl (K.W.)
* Correspondence: mateusz.marcinkowski@pk.edu.pl (M.M.)

Abstract: The object of this work is to determine the correlation on the Nusselt number on the individual rows of a four-row tubular finned heat exchanger with continuous fins with a staggered tube arrangement using CFD modelling. Correlations for calculating Darcy-Weisbach friction factors on individual tube rows were also determined. Relationships for the Nusselt number and friction factor derived for the entire exchanger based on CFD modelling were compared with those available in the literature determined using experimental data. The maximum relative differences between the Nusselt number for a four-row exchanger determined experimentally and by CFD modelling are in the range from 22% for a Reynolds number based on a tube's outside diameter of 1,000 to 30% for a Reynolds number of 13,000. The maximum relative differences between the friction factor for a four-row exchanger determined experimentally and by CFD modelling are in the range of 50% for a Reynolds number based on a tube outer diameter of 1,000 to 10% for a Reynolds number of 13,000. The CFD modeling performed shows that in the range of Reynolds numbers based on hydraulic diameters from 150 to 1,400, the Nusselt number for the first row in a four-row finned heat exchanger is about 22% to 15% higher than the average Nusselt number for the entire exchanger. In the range of Reynolds number changes based on hydraulic diameter from 2,800 to 6,000, the Nusselt numbers on the first and second rows of tubes are close to each other. Correlations on Nusselt numbers and friction factors derived for individual tube rows can be used in the design of plate-fin and tube heat exchangers used in equipment such as air-source heat pumps, automotive radiators, air-conditioning systems and in air hot-liquid coolers. In particular, the correlations can be used to select the optimum number of tube rows in the exchanger.

Keywords: plate-fin and tube heat exchanger; air-side Nusselt number; different heat transfer coefficient in particular tube row; mathematical simulation; numerical simulation; CFD simulation, air heat pump

1. Introduction

Finned heat exchangers (FHE) are widely used in applications for renewable energy sources or zero-emission processes like air heat pumps or exchangers for waste energy recovery [1]. The market for that equipment is growing significantly and will be and there is continued potential for growth due to the zero-emission policy, decarbonization, degasification and geopolitical issues [2][3]. There are more and more research which discuss also about increase heat transfer rate to limit the construction materials of any type of heat exchanger [4]. The minimizing equipment has a positive effect on reducing the noise generated by the unit and the total pressure drop on the gas side [1].

So, is it also possible to minimize finned heat exchanger? Can local values of air-side heat transfer coefficient (HTC) be applied for air heat pump. Can you do the same for all finned heat exchangers?

Even though, science does not have fully understanding of FHE with their complicated phenomena on the air- and water-side [5]. Individual rows function differently. It depends on the FHE geometry and more newly developed geometries are described.

 doi:10.20944/preprints202207.0089.v1

Bošnjaković and Muhič [6] presented star fin shape of FHE. Variability are due to the different air and water temperatures and airflow vortexes and velocity. This result in different heat transfer coefficient in each row [7].

Still, there is a lot of research for experimentally or numerically determining the average HTC of FHE. Those HTCs are used in the standard designing process of FHE. Sadeghianjahromi and Wang [8] collected several dozen average HTC of FHE for different fin geometries: plain, louvre, wavy, and plain with vortex generation. This research presented a detailed review of experimental considers heat transfer and pressure drop characteristics of enhancements. Zhang et al. [9] presented experimentally determine characteristics of airfoil fin heat exchanger. The research showed that the pressure drop in the airfoil fin heat exchanger is only about 1/6 of that in the zigzag channel FHE with a comparative heat transfer rate. Average HTCs are also widely used during evaporation or condensation heat transfer. Jige et al. [10] researched the two-phase evaporation flow of FHE using thermodynamic fluids: R32 and R1234ze(E). The authors noticed that in some region of the FHE, the HTC are significantly smaller than in the rest of the FHE regions, due to the formed dry area, which decrease HTC. Vaisi et al. [11] presented heat transfer characteristics during condensation flow in FHE with two types of fins. The authors spotted also, that higher wave amplitude to wavelength ratios, lower pitch to height ratio of the fins, lower wavelength to the fin length ratios, and lower fin pitch to wave amplitude ratios are obtained a higher thermal performance factor. Xie et al. [12] presented average heat transfer correlations of FHE. They have been designated numerically, although for the large tube diameter from 16 mm to 20 mm. Currently in technique of air heat pump evaporators or generally finned heat exchangers, there is a trend to minimize tube diameter to 12 mm or even to 10 mm and 8 mm. This research showed that HTC is dropped down as the tube diameter increases. Kim et al. [13] experimentally researched Colburn factors of FTE for large fin pitch from 7.5 mm to 15 mm. It turn out that j-factor is higher for fin pitch 15 mm that for fin pitch 7.5 and surprisingly this experiment showed that average j-factor for four row FHE is higher than for eight row FHE.

Studies are appearing that involve local HTC of FHE. These studies usually describe the local heat exchange and often compare it to the average HTC. Che and Elbel [14] showed the experimental and numerical determination of heat transfer coefficients (HTCs) using the absorption-based mass transfer method. This study showed that the HTC value in the first row of FHE compared to the second row of FHE can be 30% higher. Węglarz et al. [15] presented a new analytical method for the thermal calculation of FHE. This method can use individual or average correlation of HTC, Nusselt number or Colburn factor. Marcinkowski et al. [16] compared individual rows of tube air-side Nusselt numbers to average HTC in the entire FHE. This investigation showed that the heat flow rate transferred in the first rows of tubes can reach up to 65% of the heat output of the entire exchanger.

The aims of the current study is to numerically investigate local HTC and local pressure drops though Nusselt number and Darcy-Weisbach (D-W) friction factor determination. The geometry of the FHE was selected currently the most common dimensions in engineering for tube diameters, fin pitch, fin thicknesses and longitudinal and transverse tube pitch (Tab. 1). Similar geometries and air speed ranges were analyzed by Wang et al. [17] and Wang et al. [18]. The limitations of the compared study are presented in Table 3. Both studies investigated experimentally average j and f factors. First study [17] compare correlations for dry and wet conditions. The authors conclude that the sensible j factors under dehumidifying conditions are not dependent on inlet air parameters. Furthermore, they showed that in the case of a completely wet surface, the f factors do not change as a function of the inlet air parameters and, moreover, change slightly as a function of the fin pitch and the number of tube rows. Second study [18] presented semi universal correlation which considers not only Reynolds number, but also the fin pitch, fin thickness, the outer tube diameter and the number of tube rows.

Although the above mentioned researches has been studied in detail, insufficient attention has been paid to local air flow behavior as Nusselt number and Darcy Weisbach

 doi:10.20944/preprints202207.0089.v1

friction factor correlations. Especially, for the FHE which are currently used in engineering. The paper present not only the correlations, but also simple, easily repetitive method to determine those correlations (Fig. 4).

2. Problem Statement and Data Reduction

This research shows a steady-state and three-dimensional (3D) computational fluid dynamics (CFD) simulation. The main assumptions are:

- Fixed inlet air temperature: 20 °C.
- Air outlet opening condition - control of medium mass air temperature in the outlet section.
- Fixed air-side fins and tubes temperature: 70 °C.
- Air parameters variable as a function of temperature.
- Reynolds-Averaged Navier-Stokes equations of the mass, momentum, and energy conservation were used
- Shear Stress Transport turbulence model.
- The residuals were set to less than 10^{-3} for the continuity equations and 10^{-5} for the energy equations, respectively, to ensure that the calculations converge.
- The simulations were done by ANSYS-CFX 2020 R2 software.

The mathematical model is based on the hydraulic diameter d_h, which is calculated using the definition proposed by Kays and London [19] and maximum air velocity v_{max} in the minimum cross-section area A_{min}. The hydraulic diameter (Equation (1)) has been calculated by assumption dividing the volume through which air flows in one row (Equation (2)) by the surface area in contact with the air (Equation (3)).

$$d_h = \frac{4V_o}{A} \tag{1}$$

$$V_o = V_a - V_t \tag{2}$$

$$A = A_f + A_t \tag{3}$$

The symbol V_o designates the volume through which air flows in one row. The symbol A denotes total area in one row. Other symbols represent: V_a the total volume of one row, V_t the volume of tube in one row, A_f the fin area in one fin pitch, A_t the bare tube area in one row between two next fins.

$$V_a = p_l p_t (s - \delta_f) \tag{4}$$

$$V_t = \pi \left(\frac{d_o}{2}\right)^2 (s - \delta_f) \tag{5}$$

$$A_f = 2(p_l p_t - \left(\pi \frac{d_o}{2}\right)^2) \tag{6}$$

$$A_t = \pi d_o (s - \delta_f) \tag{7}$$

The symbol p_l denotes the longitudinal fin pitch, the symbol p_t designates the transverse fin pitch. Ither symbol represent: s the fin pitch, δ_f the fin thickness, d_o the outer tube diameter.

Equation (8) shows the full form of Equation (1) including Equation (4)(5)(6)(7). The most often, the hydraulic diameter in the case of FTHE is a slightly smaller than double fin pitch, and using geometry from Figure 1, equals 5.35 mm.

Preprints (www.preprints.org) | NOT PEER-REVIEWED | Posted: 6 July 2022 doi:10.20944/preprints202207.0089.v1

$$d_h = \frac{4\left(s-\delta_f\right)\left(p_l p_t - \pi\left(\frac{d_o}{2}\right)^2\right)}{2\left(p_l p_t - \left(\pi\frac{d_o}{2}\right)^2\right) + \pi d_o\left(s-\delta_f\right)} \tag{8}$$

The symbol w_{max} is given by Equation (6). Parameter w_{max} has been calculated for the minimum airflow cross-section between tubes and it can exist in a different place in case of different PFTHE construction (Figure 1).

$$w_{max} = \frac{(s \cdot p_l)}{(s-\delta_f)\cdot(p_l - d_{o,min})} \cdot \frac{(\overline{T}_a^i)}{(\overline{T}_{a,o})} \cdot w_o \tag{9}$$

The symbol w_{max} denotes the air velocity in the minimum cross-section of the air flow. The symbol $d_{o,min}$ the minimum dimension between tubes, $\overline{T}_a^i$ the mass average air temperature in *i*-th row of FTHE, $\overline{T}_{a,o}$ the inlet mass average air temperature and w_o the air velocity in front of the FTHE.

Reynolds numbers ($Re_{d_h,a}$) (Equation (10) calculated using the hydraulic diameter (d_h) (Equation (8)) and the maximum air velocities (w_{max}) (Equation (9)) for each row separately. Separate calculations were done due to the different maximum air velocities in each row of tubes caused by the higher air temperature. As a consequence the higher air temperatures is increasing air volumes in each row of tubes.

$$Re_a = \frac{w_{max} \cdot d_h}{\nu_a} \tag{10}$$

The symbols in Equation (10) are as follows: Re_a is the Reynolds number based on the air hydraulic diameter; d_h is the air hydraulic diameter; ν_a is the air kinematic viscosity.

3. Mathematical Modelling and CFD Domain

Table 1 shows data set of the materials and dimensions of the modelled FHE. The fin pitch s of FHE equals 3 mm. However, a width of the modelled air volume contains only a half of them 1.5 mm and it is reduced by the thickness of half a fin 0.07 mm. Where fin thickness δ_f equals 0.14 mm. So the modelled width is 1.43 mm. The following simplifications are allowed due to the air symmetry from third directions: top, bottom and side. The tube outer diameter d_o equals 12 mm. The transversal tube pitch is 32 mm. However, height of the modelled volume equals $0.5\,p_t = 16\ mm$, also due to the air symmetry. The longitudinal tube pitch is 27.71 mm, also the length of the each row equals 27.71 mm Fig. 1).

Table 1. Dimensions of the modelled FHE.

Description	Designation	Value
Rows	-	4
Transversal tube pitch	p_t	32 mm
Longitudinal tube pitch	p_l	27.71 mm
Tube outer diameter	d_o	12 mm
Fin pitch	s	3 mm
Fin thickness	δ_f	0.14 mm
Fin length of single row	L_r	27.71 mm

Figure 1 presents a repetitive segment of the air between one fin pitch in analysed FHE. Figure 1 shows also extended inlet and outlet zone, which is necessary for correct model for upstream and downstream pressure fields [20]. Multiple researches that show

Preprints (www.preprints.org) | NOT PEER-REVIEWED | Posted: 6 July 2022 doi:10.20944/preprints202207.0089.v1

the results of CFD modelling also include extended inlet and outlet zones. However, relating them to the different parameters such as: tube outer dimension d_o [20], fin spacing s and longitudal tube pitch p_l [21], channel height (0.5 p_t) [22], length of the tube bank (flow length) [23][24]. This paper adopted the following values, the inlet zone equals 0.5 p_t = 16 mm and the outlet zone is 1.5 p_t = 48 mm. Where the tube bank of four rows equals 110.84 mm.

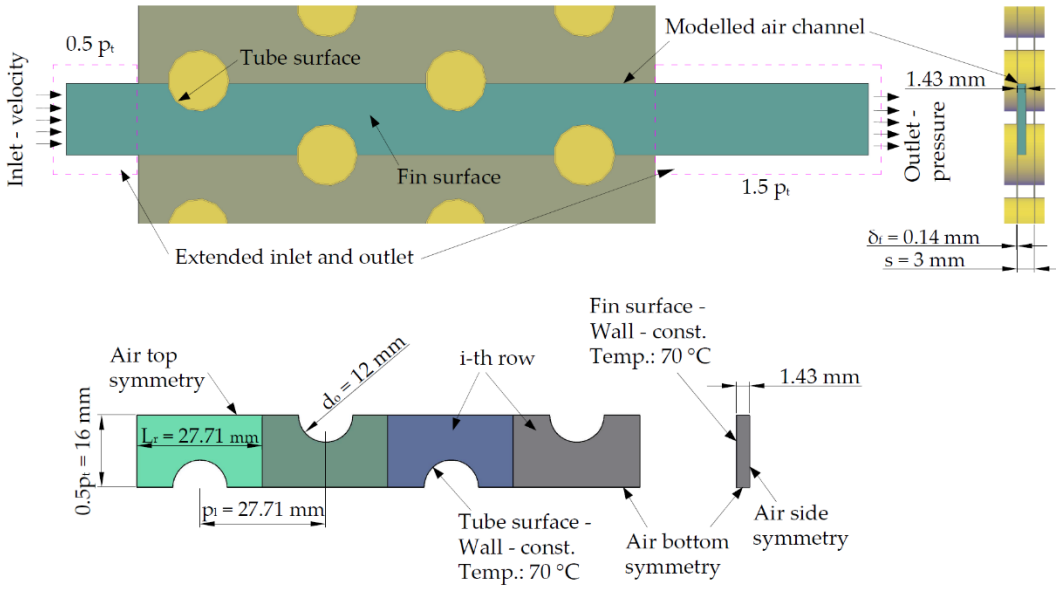

Figure 1. Repetitive fragment of the FHE: modelled channel, boundary conditions and geometry, mm.

The boundary conditions of the CFX software are shown in Figure 1. Air Inlet is set as a constant temperature: 20 °C. Air outlet is set as an opening condition with verification mass average temperature in the outlet cross section of the air. The modelled air zone have symmetry conditions from the top, bottom and side. Wall boundary conditions is set on the opposite surface (fin surface) from the air symmetry side. This boundary conditions is marked by constant temperature: 70 °C. The same conditions with the same constant temperature are set on the tube surfaces. The different constant temperature of the fin and tubes surface in range from 60 °C to 80 °C cause a slight discrepancies, less than 1.6% compare to the constant temperature in current study: 70 °C [16]. The proposed conditions are universal and they can be used in water to air finned heat exchange where we have changing fluid and gas temperature, and also in evaporator or condenser, where we have constant temperature of phase transition and on the other side changing temperature of fluid or gas, what is most commonly used in air heat pumps or air conditioning.

Preprints (www.preprints.org) | NOT PEER-REVIEWED | Posted: 6 July 2022 doi:10.20944/preprints202207.0089.v1

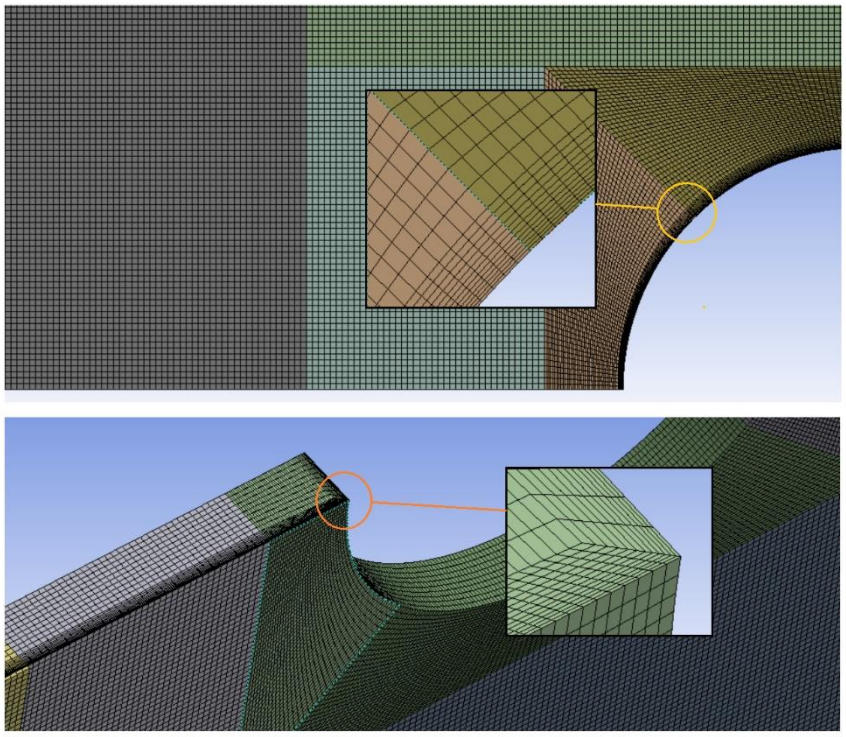

Figure 2. Repetitive fragment of the FHE with finite element mesh.

Figure 2 presents finite element mesh of the repetitive fragment of the modelled FHE. The mesh has been divided into couple of volumes for better arrangement into equal parts. Particular colours in the figure 2 present this division. Additionally, the compaction of the mesh has done at the fin and tubes surfaces. The compaction is shown in zoom windows in figure 2. The regularity of the volumes are disturbed in the compaction zone, because elements are extended and inclined. However, deformation of the volumes is within acceptable limits. The minimum orthogonal angle is 35.6°. The mesh expansion factor equals 14 and the maximum aspect ratio is 22.

4. Mesh Parameters and Mesh Independent Study

Table 1 presents a calculation mesh data. The calculation mesh consist of the cuboid elements only. Additionally, in order to increase accuracy of the simulations, it has densities at the boundary between the air and the fins and tubes (Figure 2b). Densities are as a first layer thickness with 1.1 growth rate and 12 number of the layers.

Table 2. Mesh data for the modelled part of the heat exchanger (Figure 2b).

Finite Elements Number	**3,104,268**
Number of nodes	3,277,429
Dimension of the element, mm	0.15
Maximum dimension of the element, mm	0.20
Boundary layer	First layer thickness: 0.023mm ($y^+ = 1$) Growth rate: 1.1 Number of layers: 12
Minimum orthogonal angle	Air: 35.6°
Mesh expansion factor	Air: 14
Maximum aspect ratio	Air: 22

Preprints (www.preprints.org) | NOT PEER-REVIEWED | Posted: 6 July 2022 doi:10.20944/preprints202207.0089.v1

The mesh independent study was done for all CFD simulations for the entire range of air velocity, separately for all air velocities. Designation of Nusselt number stabilization has been done by calculation of relative differences (e_{Nu}) between different Nusselt number in the fourth row of FHE for mesh with particular element numbers (Nu_{n_i}) and the reference Nusselt number in the fourth row of PFTHE for mesh with 3,104,268 mesh elements ($Nu_{3,104,268}$) are as follows $e_{Nu} = \frac{(Nu_{n_i} - Nu_{3,104,268})}{Nu_{3,104,268}}$.

Nusselt number stabilisation for air velocity—10 m/s in front of the heat exchanger for the fourth row of FHE is shown in Figure 3. Acceptable Nusselt number stabilization has been reached for mesh with 3,104,268 elements. Continuing to increase mesh elements does not provide significantly stable results and the relative differences for the mesh with the highest number elements is differ less than 1.6 %. The discrepancies for other rows of FHE and the lower air velocities are even close to 0. This shows that, in the considered scenario, the greatest irregularity of flow and turbulence exists in the last row of FHE.

The calculation time has been also shown in Figure 3. It can be observed that chosen mesh has more than double the calculation time compare to the mesh with the highest number of elements. The above reference mesh has been selected for further calculations as the best ratio of calculation accuracy to calculation time.

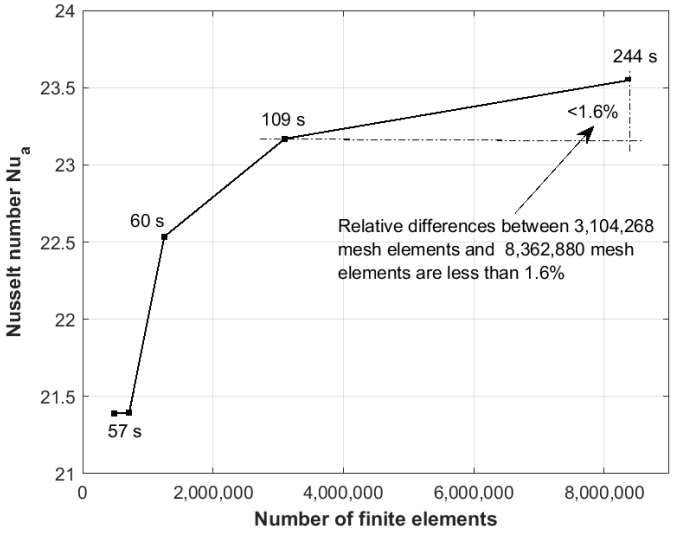

Figure 3. Nusselt number stabilisation for mesh independent study from the fourth row of FHE for 10 m/s air velocity in front of the heat exchanger.

A mesh with 3,104,268 elements was selected. Mesh elements' size belongs to the following mesh sizes: mesh element size: 0.15 mm; mesh max size: 0.20 mm (Table 2). The whole mesh contains cuboidal elements only (Figure 2).

5. CFD Model Validation

The results of the Nusselt number and D-W friction factor of the investigated CFD model are compared with recent correlations such as Wang et al. [18] and Wang et al. [17]. Fig. 4 shows the air-side Nusselt and the air-side D-W friction factor as a function of Reynolds number.

Preprints (www.preprints.org) | NOT PEER-REVIEWED | Posted: 6 July 2022 doi:10.20944/preprints202207.0089.v1

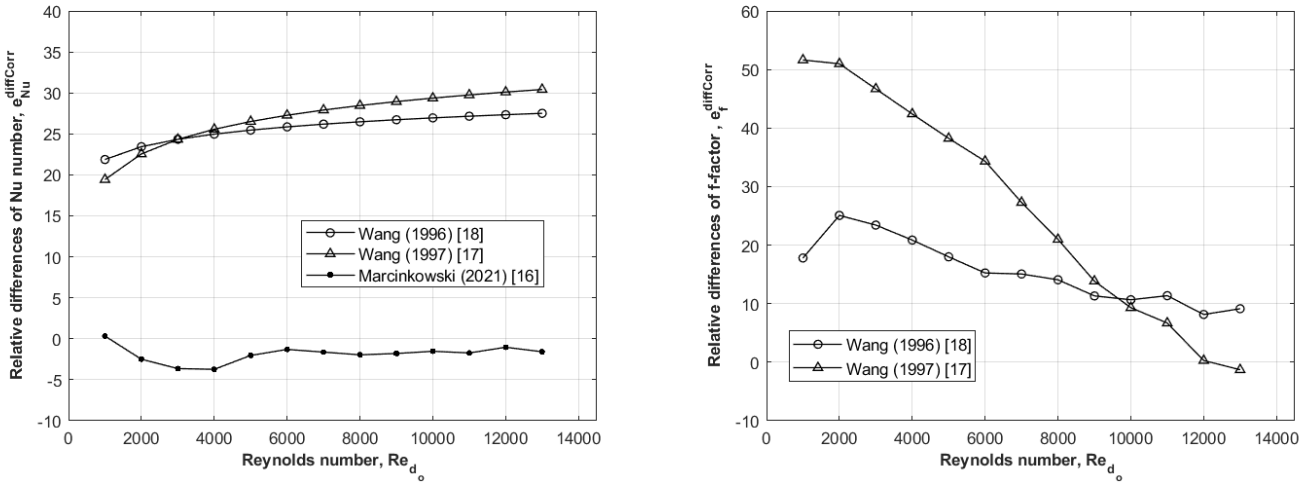

(**a**) (**b**)

Figure 4. The relative differences calculated using different correlations of (a) Nusselt number for the entire FHE; (b) Darcy-Weisbach friction factor for the entire FHE.

Figure 4a compares the correlations determined by the current study with Wang et al. [18], Wang et al. [17] and Marcinkowski et al. [16] in case of Nusselt number comparison. Table 3 presents geometry dimensions of the compared studies. It can be noticed that all presented research have similar geometries.

Table 3. Dimensions of the FHE geometry from different research.

Description	Designation	Current study	Wang et al. [18]	Wang et al. [17]
Rows	-	4	2-6	2-6
Transversal tube pitch [mm]	p_t	32.00	25.40	25.40
Longitudinal tube pitch [mm]	p_l	27.71	22.00	22.00
Tube outer diameter [mm]	d_o	12.00	10.23	10.23
Fin pitch [mm]	s	3.00	1.75-3.21	1.82-3.20
Fin thickness [mm]	δ_f	0.14	0.13-0.2	0.13
Fin length of single row [mm]	L_f	27.71	22.00	22.00

The relative differences between the current study and the other correlations were defined as: $e_{param}^{diffCorr} = 100(param^{diffCorr} - param^{Present})/param^{diffCorr}$, where superscript diffCorr indicates that it is the value of a given study: Wang et al. [18], Wang et al. [17] and Marcinkowski et al. [16]. The subscript param means the following parameters: Nu number and j-factor.

The relative difference between the Nusselt number presented in this study and the Nusselt number correlation for Wang et al. [18], is 21.87 % for Re_{d_o} = 1000 and 27.51 % for Re_{d_o} = 13,000 (Figure 4a). The relative difference between the Nusselt number presented in this study and the Nusselt number correlation for Wang et al. [17], is 19.42 % for Re_{d_o} = 1000 and 30.42 % for Re_{d_o} = 13,000 (Figure 4a). The relative difference between the Nusselt number presented in this study and the Nusselt number correlation for Marcinkowski et al. [16] is -3.6 % for Re_{d_o} = 3,000, 0.33 % for Re_{d_o} = 1,000 and -1.58 % for Re_{d_o} = 13,000 (Fig. 4a). The results of Marcinkowski et al. [16] were performed by CFD modelling using Ansys CFX software. The current study was performed for the same mathematical model. The only difference for the range of the Nusselt number test is due to the use of Ansys Fluent.

Figure 4b compares the correlations determined by the current study with Wang et al. [18], Wang et al. [17] in case of D-W friction factor comparison.

The relative difference between the friction factor correlation presented in this study and the friction factor correlation for Wang et al. [18], is 17.8 % for Re_{d_o} = 1000 and 9.13

Preprints (www.preprints.org) | NOT PEER-REVIEWED | Posted: 6 July 2022 doi:10.20944/preprints202207.0089.v1

% for Re_{d_o} = 13,000 (Figure 4b). The relative difference between the friction factor correlation presented in this study and the friction factor correlation for Wang et al. [17], is 51.62 % for Re_{d_o} = 1000 and -1.29 % for Re_{d_o} = 13,000 (Figure 4b).

The above results in Figure 4a and Figure 4b show that the developed model and calculations performed in Ansys Fluent fairly accurately reproduce the heat transfer assumptions in the heat exchangers discussed. The slight differences may be due to the fact that the correlation presented in this work was determined using CFD modelling, while the other correlations were determined using experimental tests. The differences between the correlations obtained experimentally and the correlation determined by Ansys Fluent calculations are acceptable (Figure 4), given that the geometries of the exchangers analysed differ both in tube diameter and in the spacing of tubes and fin fins. Also, different experimental test conditions and the conditions adopted in the CFD modelling can cause differences in the values of the Nusselt number and the friction coefficient.

6. Method of Determining HTC on the Individual FHE Row

Determination of the HTCs, Nusselt numbers, Colburn factors for the individual rows is illustrated in Figure 4. The method uses constant fin and tube temperatures (70 °C). Previous paper of Marcinkowski et al. [16] shows also simulations for constant fin and tube temperatures: 60 °C and 80 °C. The determined HTCs do not differ more than 1.5% for different constant surface temperatures of the tubes and fins. The simplicity of this method means that it can be used in practice.

Determining HTC, Nusselt number and Colburn factor:

- Extract the average mass flow temperature $\bar{T}^{i}{}_{a}$ from the Fluent Post-Processor of the air velocity for every row separately. Areas to extract the average mass flow temperatures are in a half distance between the next two tubes in rows.
- Compute the difference of the average logarithmic temperature ($\Delta\bar{T}_{m,a}$) between the fin and the tube surface temperature (T_w) and the average mass flow temperature ($\bar{T}_a^i$) (Eq. (3)).

$$\Delta\bar{T}_{m,a} = \frac{(T_w - \overline{T}_a^{i+1})(T_w - \overline{T}_a^{i})}{ln(\frac{T_w - \overline{T}_a^{i+1}}{T_w - \overline{T}_a^{i}})} \tag{11}$$

The symbol T_w means the constant fin and tube surface temperature. The symbols $\bar{T}_a^i$ and $\bar{T}_a^{i+1}$ denotes the inlet and outlet mass average air temperature for the *i*-th row of FTHE.

- Extract the total heat flow transferred from the fin and the tube wall surface to the air for the *i*-th row of the FTHE (Figure 4).
- Compute the individual HTC for each row separately (Eq. (4)).

$$\alpha_a^i = Q_i/(A_w \Delta T_{m,a}^i) \tag{12}$$

The symbol Q_i means the total heat flow for the individual row for the *i*-th row of the FTHE; α_a^i denotes the air-side HTC for the *i*-th row of the FTHE.

- Compute the Nusselt number (Eq. (5)) and the Colburn factor (Eq. (6)).

$$Nu_a^i = (\alpha_a^i\, d_h)/\lambda_a \tag{13}$$

Determining friction factor:

- Extract the average value of static pressure $\Delta\bar{p}_a^i$ from the Fluent CFD-Post of the air velocity for every row separately. Areas to extract the average value of the static pressure are in a half distance between the next two tubes in rows.
- Compute the individual Darcy-Weisbach friction factor for each row separately (Eq. (14)).

Preprints (www.preprints.org) | NOT PEER-REVIEWED | Posted: 6 July 2022 doi:10.20944/preprints202207.0089.v1

$$f_a{}^i = \left(\frac{d_h \bar{\rho}_a^i}{L_r \rho_a^i}\right)\left[\frac{2\rho_a^i \Delta\bar{p}_a^{\,i}}{\bar{\rho}_a^i w_{max}^i} - (1+\sigma^2)\left(\frac{\rho_a^i}{\rho_a^{i+1}} - 1\right)\right] \quad (14)$$

The symbol d_h means hydraulic diameter (Eq. (8)), $\bar{\rho}_a^i$ denotes the arithmetic average of the air density for the *i*-th row of the FHE; ρ_a^i means the inlet air density, ρ_a^{i+1} means the inlet air density, L_r designated the length of the considered volume, w_{max}^i designated the maximum air velocity (Eq. (9) for the *i*-th row of the FHE. The other symbols mean: $\Delta\bar{p}_a^{\,i}$ denotes the average air pressure drop for the i-th row of FHE, σ designated ratio of the fin pitch cross section and two next fins distance cross section area.

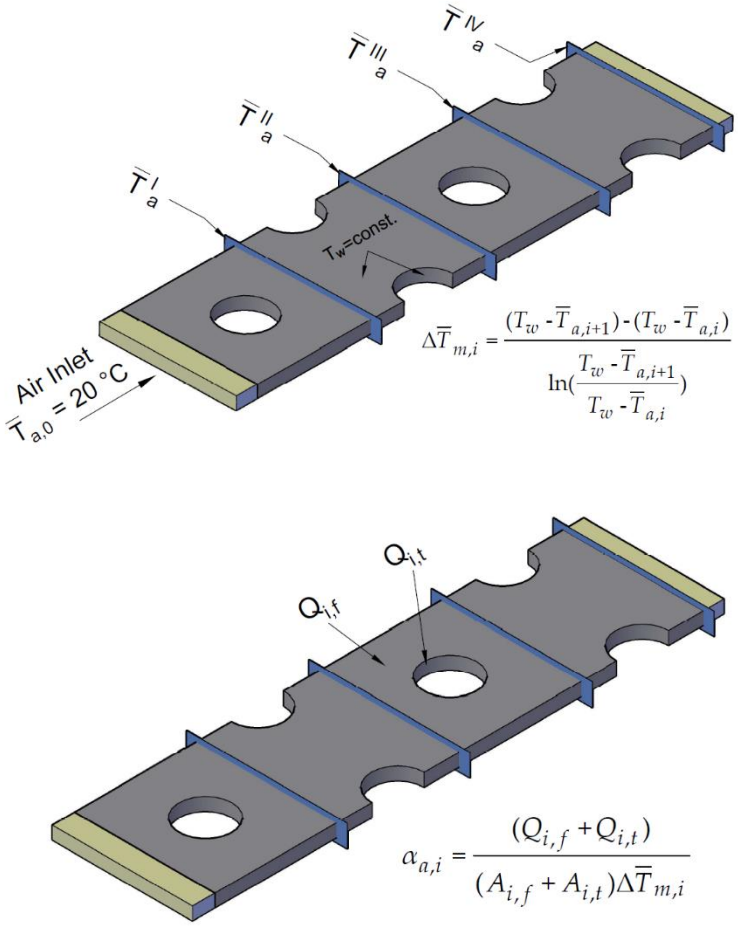

Figure 4. Graphical representation of determining HTC on the individual row based on a CFD simulation.

7. Results and Discussions

Figure 5 and Figure 6 presents results of Nusselt number and D-W friction factor for both individual correlation on each row and average correlations for entire FHE. Parameter w_{max} in Equation (7) and (8) is almost double the air velocity in front of the FHE. Reynolds numbers are related to the maximum velocity, that's why Reynolds number for the same air velocity in front of the FHE has different value for the maximum air velocity of the *i*-th tube rows of FHE.

The Nusselt number function which was approximate to the modelled CFD data is presented in the Equation (7). This function contains two parameters: x_1 and x_2, which was presented in Table 4 and Table 5. The function depends on the Reynolds number and Prandl number. Equation (7) presents also range of Reynolds number and Prandtl number range.

Preprints (www.preprints.org) | NOT PEER-REVIEWED | Posted: 6 July 2022 doi:10.20944/preprints202207.0089.v1

$$Nu_a = x_1 \cdot Re_a^{x_2} \cdot Pr_a^{\frac{1}{3}} \qquad \mathrm{Re}_a = \frac{w_{\max}\ d_h}{\nu_a} \qquad \begin{matrix} 150 \le Re_a \le 5{,}900 \\ Pr_a = 0.7 \end{matrix} \tag{7}$$

The air-side Nusselt number (Nu_a) correlation (Eq. (7)) follows the Colburn relation $Nu/(RePr^{1/3}) = f(Re)$ where the function f(Re) is determined using experimental data. Having determined the coefficients x1 and x2 for the air-side Nusselt number function (Eq. (9)) by means of CFD modelling, it can be expected that the function (Eq. (7)) will also be valid for other gases. The Nusselt numbers functions for the first, second, third, fourth rows of tubes and the average Nusselt numbers function for the entire FTHE are illustrated in Figure 5. Table 4 and Table 5 shows the corresponding correlation's parameters for all function presented in Figure 5.

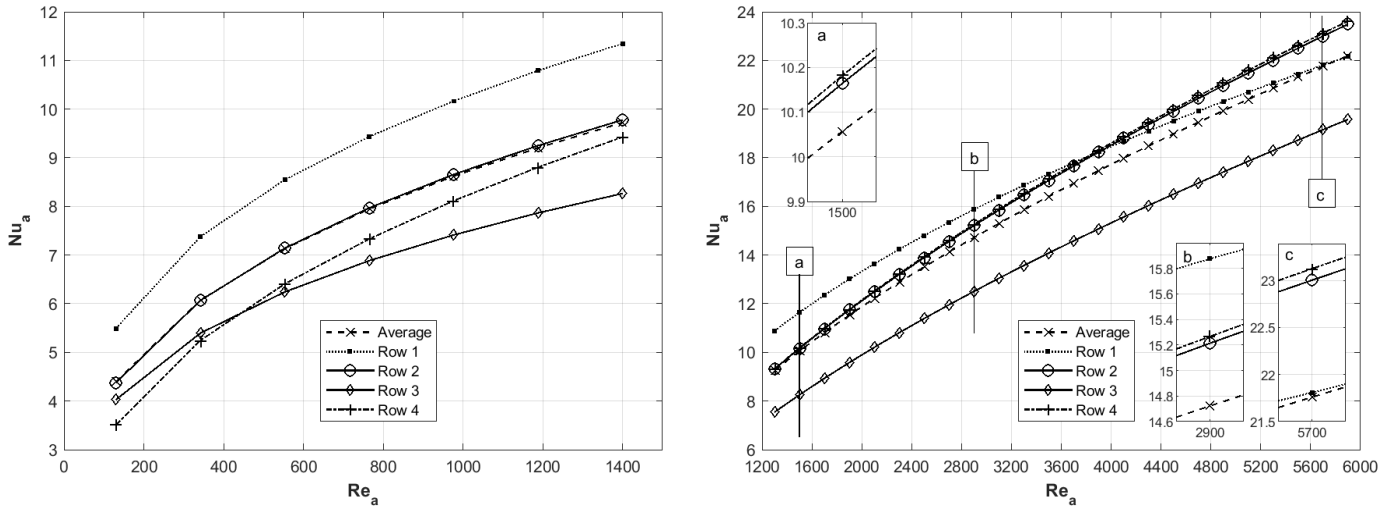

(**a**) (**b**)

Figure 5. (a) Nusselt number as a function of the Reynolds number for the individual tube rows for Reynolds number range from: (a) 150 to 1,400; (b) 1,400 to 6,000

The D-W friction factor function which was approximate to the modelled CFD data is presented in the Equation (8). The friction factor function contains two parameters: x_1 and x_2, which was presented in Table 4 and Table 5. The function depends on the Reynolds number and Prandl number. Equation (8) presents also range of Reynolds number.

$$f_a = x_1 \cdot Re_a^{x_2} \cdot \qquad \mathrm{Re}_a = \frac{w_{\max}\ d_h}{\nu_a} \qquad 150 \le Re_a \le 5{,}900 \tag{8}$$

The friction factor functions for the first, second, third, fourth rows of tubes and the average friction factor function for the entire FTHE are illustrated in Figure 6. Table 7 and Table 8 shows the corresponding correlation's parameters for all function presented in Figure 6.

Preprints (www.preprints.org) | NOT PEER-REVIEWED | Posted: 6 July 2022 doi:10.20944/preprints202207.0089.v1

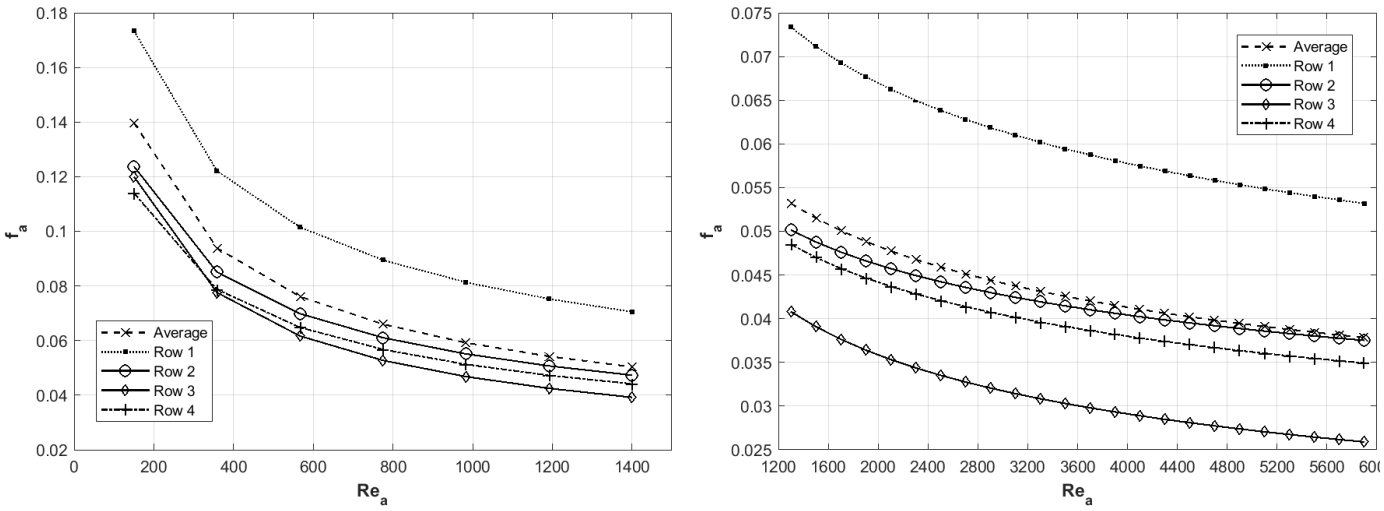

Figure 6. (a) Friction factor as a function of the Reynolds number for the individual tube rows for Reynolds number range from: (a) 150 to 1,400; (b) 1,400 to 6,000

The coefficients x_1 and x_2 for each correlation was calculated considers the 95% confidence intervals limits for the Nusselt numbers which are determined by the least-squares method. The values of the Nusselt number calculated for a given Reynolds number (Equation (7)) differ by +/− 2 σ. The σ symbol means the mean standard deviation of the Nusselt numbers obtained by the CFD modelling. Determination of 95% confidence intervals for Nusselt number correlations received at by least-squares is described at Chapter 11 of Taler's book [24].

Table 4. Air side Nusselt number correlation parameters of FTHE for Reynolds number range from 150 to 1,400.

	Nusselt number correlations	Friction factor correlations
Average	$Nu_a = 0.9760\ Re_a^{0.3337}\ Pr_a^{1/3}$	$f_a = 1.3788\ Re_a^{-0.4569}$
Row 1	$Nu_a = 1.4001\ Re_a^{0.3053}\ Pr_a^{1/3}$	$f_a = 1.3051\ Re_a^{-0.4028}$
Row 2	$Nu_a = 0.9478\ Re_a^{0.3386}\ Pr_a^{1/3}$	$f_a = 1.0700\ Re_a^{-0.4305}$
Row 3	$Nu_a = 1.0403\ Re_a^{0.3025}\ Pr_a^{1/3}$	$f_a = 1.4770\ Re_a^{-0.5010}$
Row 4	$Nu_a = 0.5230\ Re_a^{0.4156}\ Pr_a^{1/3}$	$f_a = 0.9585\ Re_a^{-0.4249}$

Table 5. Air side Nusselt number correlation parameters of FTHE for Reynolds number range from 1,400 to 6,000.

	Nusselt number correlations	Friction factor correlations
Average	$Nu_a = 0.1652\ Re_a^{0.5781}\ Pr_a^{1/3}$	$f_a = 0.2673\ Re_a^{-0.2251}$
Row 1	$Nu_a = 0.4217\ Re_a^{0.4700}\ Pr_a^{1/3}$	$f_a = 0.3370\ Re_a^{-0.2127}$
Row 2	$Nu_a = 0.1305\ Re_a^{0.6118}\ Pr_a^{1/3}$	$f_a = 0.1983\ Re_a^{-0.1917}$
Row 3	$Nu_a = 0.0923\ Re_a^{0.6307}\ Pr_a^{1/3}$	$f_a = 0.3523\ Re_a^{-0.3006}$
Row 4	$Nu_a = 0.1282\ Re_a^{0.6145}\ Pr_a^{1/3}$	$f_a = 0.2303\ Re_a^{-0.2173}$

7. Conclusions

The new air-side correlations of the Nusselt number and the D-W friction factor proposed for the four-row FHE. The individual correlations on the individual rows of the FHE can significantly improve a construction of the FHEs. This paper present the analysed range of the air velocities in the front of the heat exchanger from 0.5 m/s to 10 m/s. Both the Nusselt number correlations and the D-W friction factors for modelled FHE (Fig. 1) have been developed using the CFD software – Ansys 2020 R2 Fluent. The newly determined individual correlations (Tab. 4 and Tab. 5) for a dedicated rows are considerably

 doi:10.20944/preprints202207.0089.v1

different from the average correlations of the Nusselt numbers and the D-W friction factors (Fig. 5 and Fig. 6). The conclusions are as follows:

1. The results of the comparison the current data with author's previous data are almost identical. The relative differences for the entire Reynolds number range is maximum 3,6% (Figure 5). The important information is that current data was calculated using Ansys 2020 R2 Fluent software, however the previous author's data was determined using Ansys 2020 R2 CFX software.
2. The Nusselt numbers and friction factors data are the highest value for the first row of the FHE, due to the maximum temperature difference between air and fin and tube surface and the fewest dead zones (Fig. 5 and Fig. 6).
3. The obtained Nusselt number and friction number correlations showed that the third row is the least efficient. The Nusselt numbers and friction factors falls to the third row and then increases in the fourth row for the entire air velocity range This could mean that air stream in the penultimate row is the least turbulent or air stream develops a narrow flow channel. The rest of the volume creates broad dead zones in front of and behind the tubes in the third row (Figure 5 and Figure 6).
4. The Nusselt number for the fourth row has the minimum value for the Reynolds number equals 150. However, it changes and the Nusselt number for the fourth row has the maximum value for the Reynolds number equals 6000.
5. The greater the Reynolds number for the range tested, the more the Nusselt number values for the first row converge to the average value for the entire FHE. Moreover, the higher the Reynolds number for the range tested, the more the Nusselt values for the second and the third row values equalise and increase from the mean value for the entire FHE.
6. The values of the friction factor for a given row of tubes are more stable and almost do not change their position in the entire range of the Reynolds numbers. The exception is the fourth row, which overtakes the third row at a Reynolds number of 300.
7. Experimental verification of derived CFD-based correlations has not been carried out in this research. However, it is planned as an extension of this study. The future of this research topic also considers a wider Reynolds number range. different tube and fin pitches and tube diameters.
8. The research also showed the clear and accessible method for the determination of the Nusselt number and friction factor correlation for individual rows which can reduce or even completely eliminate an expensive experimental research.
9. The CFD simulation must be precisely conducted with a proper finite volume mesh and turbulence model for turbulent flows. CFD modelling is an effective tool for determining individual correlations for calculating the air-side Nusselt number on the individual tube rows of the exchanger.
10. This method can be used not only for designing water to air or air to water FHE like coolers and heaters in air-conditioning or other finned heat exchangers in heat recovery, but also for phase changing fluid to air and air to phase changing fluid FHE like evaporators and condensers in air heat pump, cooling and refrigeration process.

Author Contributions: Conceptualisation. D.T.. J.T.; methodology. software. validation. formal analysis. investigation. writing—original draft preparation. M.M.; resources. data curation. M.M.. K.W.; writing—review and editing; supervision. D.T.. J.T. All authors have read and agreed to the published version of the manuscript.

Funding: This research was funded by the National Centre for Research and Development. programme: "Applied Research" implemented under The Norwegian Financial Mechanism 2014-2021: grant number NOR/SGS/MECHEX/0080/2020.

Institutional Review Board Statement: Not applicable.

Informed Consent Statement: Not applicable.

Preprints (www.preprints.org) | NOT PEER-REVIEWED | Posted: 6 July 2022 doi:10.20944/preprints202207.0089.v1

Data Availability Statement: The data presented in this study are available on request from the corresponding authors.

Conflicts of Interest: The authors declare no conflict of interest.

Nomenclature

$A = A_w$	total surface area (fin and tube outer surface area), m²
A_f	fin surface area, m²
A_{min}	minimum air flow area, m²
A_t	outer tube area, m²
CFD	Computational Fluid Dynamics
$D-W$	Darcy – Weisbach (friction factor)
$diffCorr$	different correlation, eg. Wang et al. or Marcinkowski et al.
d_h	hydraulic diameter, m
d_o	outer tube diameter, m
$d_{o,min}$	the minimum dimension between tubes, m
e	relative differences, %
f	Darcy – Weisbach friction factor
FHE	Finned Heat Exchanger
HTC	Heat Transfer Coefficient
$L_r = p_l$	length of single row, m
n	number of mesh elements
Nu_a	Nusselt number based on the hydraulic diameter
Nu_{d_o}	Nusselt number based on the outer diameter of the tube
Nu_{n_i}	Nusselt number for mesh with particular element numbers n
$Nu_{3,104,268}$	Nusselt number for mesh with 3,104,268 mesh elements
$param$	Considered parameter: Nusselt Number or D-W friction factor
$\Delta\bar{p}_a$	average air pressure drop, Pa
p_t	longitudinal fin pitch, m
p_l	transversal fin pitch, m
Pr_a	Prandtl number
s	fin pitch, m
Re_a	Reynolds number based on the hydraulic diameter
Re_{d_o}	Reynolds number based on the outer diameter of the tube
$\bar{T}_a$	mass average air temperature, °C
$\Delta\bar{T}_{m,a}$	log mean temp. difference, °C
T_w	constant wall temperature, °C
w	air velocity, m/s
V_a	total volume of one row or entire FHE, m³
V_o	volume through which air flows, m³
V_t	volume of tube in one row or in entire FHE, m³
Q	total heat transfer, W
Q_f	total heat transfer of fin, W
Q_t	total heat transfer of tube, W
x_1	Nusselt number parameter
x_2	Nusselt number parameter
y^+	dimensionless wall distance

Greek Symbols:

α	heat transfer coefficient, W/(m²·K)
δ_f	fin thickness, m
λ	thermal conductivity, W/(m·K)
ν	kinematic viscosity, m²/s
ρ	air density in i-th row cross section, kg/m³
$\bar{\rho}$	arithmetic average of the air density for i-th row, kg/m³
σ	ratio of the fin pitch cross section and two next fins distance cross section area
σ_{msd}	mean standard deviation

Subscripts:

a	air

 doi:10.20944/preprints202207.0089.v1

f	fin
i	the inlet of the *i*-th tube row
$i+1$	the inlet of the (*i*+1)-th tube row
max	maximum
t	tube
0	air inlet

Superscripts:

I, II, III and IV	number of FHE row
$Present$	data/correlation from the present research

References

1. McQuistion, F.C.; Parker, J.D.; Spitler, J. *Heating, Ventilating, and Air Conditioning Analysis and Design*, 6th ed.; JohnWiley & Sons: Hoboken, NJ, 2005.
2. Menegazzo, D.; Lombardo, G.; Bobbo, S.; De Carli, M.; Fedele, L. State of the Art, Perspective and Obstacles of Ground-Source Heat Pump Technology in the European Building Sector: A Review. *Energies* **2022**, *15*, 1-25.
3. Marina, A.; Spoelstra, S.; Zondag, H.A.; Wemmers, A.K. An estimation of the European industrial heat pump market potential. *Renew. Sustain. Energy Rev.* **2021**, *139*, 1-14.
4. Moon, H.; McGregor, D.J.; Miljkovic, N.; King, W.P. Ultra-power-dense heat exchanger development through genetic algorithm design and additive manufacturing. *Joule* **2021**, *5*, 3045–3056.
5. Thulukkanam, K. *Heat Exchanger Design Handbook*, 2nd ed.; CRC Press: Boca Raton, FL, USA, 2013.
6. Bošnjaković, M.; Muhič, S. Numerical Analysis of Tube Heat Exchanger with Trimmed Star-Shaped Fins. *Appl. Sci.* **2022**, *12*, 1-14.
7. Taler, D.; Taler, J.; Trojan, M. Thermal calculations of plate–fin–and-tube heat exchangers with different heat transfer coefficients on each tube row. *Energy* **2020**, *203*, 1-14.
8. Sadeghianjahromi, A.; Wang, C.C. Heat transfer enhancement in fin-and-tube heat exchangers – A review on different mechanisms. *Renew. Sustain. Energy Rev.* **2021**, *137*, 1-42.
9. Zhang, J.; Liu, J.; Zhang, L.; Liu, Q.; Wu, Q. Air-side heat transfer characteristics under wet conditions at lower ambient pressure of fin-and-tube heat exchanger. *Int. J. Heat Mass Transf.* **2019**, *142*, 1-8.
10. Jige, D.; Sugihara, K.; Inoue, N. Evaporation heat transfer and flow characteristics of vertical upward flow in a plate-fin heat exchanger. *Int. J. Refrig.* **2022**, *133*, 165–171.
11. Vaisi, A.; Javaherdeh, K.; Moosavi, R. Condensation heat transfer performance in multi-fluid compact heat exchangers with wavy and strip fins. *Int. J. Heat Mass Transf.* **2022**, *182*, 1-16.
12. Xie, G.; Wang, Q.; Sunden, B. Parametric study and multiple correlations on air-side heat transfer and friction characteristics of fin-and-tube heat exchangers with large number of large-diameter tube rows. *Appl. Therm. Eng.* **2008**, *29*, 1-16.
13. Kim, Y.; Kim, Y. Heat transfer characteristics of flat plate finned-tube heat exchangers with large fin pitch. *Int. J. Refrig.* **2005**, *28*, 851–858.
14. Che, M.; Elbel, S. Comparison of Local and Averaged Air-Side Heat Transfer Coefficients on Fin-and-Tube Heat Exchangers Obtained With Experimental and Numerical Methods. *J. Therm. Sci. Eng. Appl.* **2022**, *14*, 1-13.
15. Węglarz, K.; Taler, D.; Jaremkiewicz, M.; Taler, J.; Marcinkowski, M. Analytical-numerical method for calculating cross-flow tube heat exchangers considering temperature-dependent fluid heat capacities. *Int. J. Heat Mass Transf.* **2022**, *183*, 1-14.
16. Marcinkowski, M.; Taler, D.; Taler, J.; Węglarz, K. Thermal Calculations of Four-Row Plate-Fin and Tube Heat Exchanger Taking into Account Different Air-Side Correlations on Individual Rows of Tubes for Low Reynold Numbers. *Energies* **2021**, *14*, 1-13.
17. Wang, C.C.; Hsieh, Y.C.; Lin, Y.T. Performance of Plate Finned Tube Heat Exchangers Under Dehumidifying Conditions. *J. Heat Transfer* **1997**, *119*, 109–117.
18. Wang, C.C.; Chang, Y.J.; Hsieh, Y.C.; Lin, Y.T. Sensible heat and friction characteristics of plate fin-and-tube heat exchangers having plane fins. *Int. J. Refrig.* **1996**, *19*, 223–230.
19. Kays, W.; London, A. *Compact heat exchangers*. 3rd ed.; Krieger Pub Co: Malabar, FL, USA, 1998.
20. Li, H.; Zhang, S.; Ji, Y.; Sun, M.; Li, X.; Sheng, Y. The influence of catchment scale on comprehensive heat transfer performance about tube fin heat exchanger in numerical calculation. *Energy Reports* **2022**, *8*, 147–155.
21. Menéndez Pérez, A.; Fernández-Aballí Altamirano, C.; Borrajo Pérez, R. Parametric analysis of the influence of geometric variables of vortex generators on compact louver fin heat exchangers. *Therm. Sci. Eng. Prog.* **2021**, *27*, 1-11.
22. Zeeshan, M.; Nath, S.; Bhanja, D. Numerical study to predict optimal configuration of fin and tube compact heat exchanger with various tube shapes and spatial arrangements. *Energy Convers. Manag*. **2017**, *148*, 737-752.
23. Zhao, L.; Gu, X.; Gao, L.; Yang, Z. Numerical study on airside thermal-hydraulic performance of rectangular finned elliptical tube heat exchanger with large row number in turbulent flow regime. *Int. J. Heat Mass Transf.* **2017**, *114*, 1314-1330.

 doi:10.20944/preprints202207.0089.v1

24. Okbaz, A.; Pınarbas, A.; Olcay, A.B.; Aksoy, H. An experimental, computational and flow visualization study on the air-side thermal and hydraulic performance of louvered fin and round tube heat exchangers. *Int. J. Heat Mass Transf.* **2018**, *121*, 153-169.